Chapter 10

Swirl Stabilized Flame Study : Experimental Results and Analysis

Following the experimental procedures described in Chapter 9, experiments were conducted on swirl stabilized turbulent flames using bottled commercial grade methane. The experiments included both, totally and partially premixed conditions and were performed for 2 total air flow rates (Q_{Air}), 3 equivalence ratios (Φ), and 2 swirl numbers (S). This chapter presents the results, analysis and the discussion of this experimental study.

10.1 Experimental System Characterization

The present experimental rig was designed to sustain swirl stabilized turbulent flames. These flames are hydrodynamically stabilized in a three dimensional flow and temperature field. The flame (reaction zone) normally resides on the shear layers that encompass the CRZ and the ORZ. The temperature and the flow field together, determine the degree of preheating of the reactants at the inlet to the combustion chamber, caused due to the mixing of the incoming reactants and the re-circulated combustion products. They also define the flow conditions at the inlet to the reaction zone and thus, its size, shape and spatial location. The heat release occurring in the reaction zone, in turn has a strong influence on both the temperature and the flow structure within the combustion chamber. Therefore, from the

systems perspective, the reaction rates, the species profile, the flow field and the temperature field are all coupled within a closed loop system, and the dynamics of the flame front cannot be decoupled from that of the three-dimensional reaction volume, and thus the u' cannot be corrected for the spatial distance between the plane of u' measurement and the location of the flame front. Measurement of the localized velocity fluctuations at the rection zone can be accomplished using a LDV system. However, such a system was not available for this research effort.

10.1.1 Fully Premixed Combustion Experiments

To generate totally premixed conditions, the fuel was mixed with the air outside the combustor in a mixing chamber and the premixed charge was then injected into the combustor. This setup ensured that no oscillations were generated in the equivalence ratio when the flow was imparted velocity perturbations using the acoustic driver (speaker).

10.1.2 Partially Premixed Combustion Experiments

Under the partially premixed conditions, the fuel was injected into the swirling air stream within the combustor through the central fuel injection system. Thus, mixing of fuel and air occurred as the fuel-air mixture convected downstream from the injector to the flame. The degree of mixing can be varied by changing the location of the axial fuel injector. For partially premixed flames, any pressure oscillation at the plane of injection is not expected to effect the fuel injection, because the fuel injection holes being $\frac{1}{32}$" in diameter provide very high acoustic impedance. Thus, the fuel flow upstream of the injection holes is decoupled from the acoustic field present in the combustor. However, the pressure oscillations will certainly effect the air stream, and thus generate equivalence ratio oscillations. Therefore, partially premixed flames are subjected both to variation in the equivalence ratio across the cross-section of the flow and also to equivalence ratio oscillations.

10.2 Experimental Results for Fully Premixed Conditions

Experiments were conducted using 'CP grade 93 % pure methane' for Φ of 0.55, 0.6 and 0.65, Q_{Air} of 15 scfm and 20 scfm, and S of 0.79 and 1.19. The combination of these parameters resulted in 12 sets of experiments that were conducted for totally premixed inlet flow conditions. The flow rates chosen were limited primarily due to the constraints of the present exhaust system. They represent a Reynolds number of 14900 and 19800 respectively, based on the diameter of the inlet of the quarl. The swirl numbers chosen are within the range used by the land based gas turbine industry. The maximum Φ studied was limited by the present limitations of the system which controls the thermal environment of the test cell.

10.2.1 Interpretation of the Results

Figure 10.1 through Figure 10.8 show magnitude and the phase of the FRF between the OH^* chemiluminescence signal and the velocity fluctuations u' for the two flow rates and the two swirl numbers. Most experimental data discussed here is in the range of 20-380 Hz. However, at $\Phi = 0.55$ and at $\Phi = 0.6$, for $Q_{Air} = 15$ scfm, the range of the dynamic experiment was limited to 330 Hz, as there was poor coherence between the OH^* chemiluminescence and the velocity perturbations beyond 330 Hz. For Q_{Air} of 20 scfm, the range of the dynamic experiments were increased to 490 Hz to capture the effects at the acoustic mode of the rig that is seen at 460 Hz.

Figures 10.1, 10.3, 10.5, and 10.7 detail the magnitude of the FRF. These figures show that for all the experimental conditions, the response of the flame to u' perturbations behaves as a low pass filter, which is about 8^{th} order in nature. The bandwidth of the dynamic response increases with increasing Φ. For the frequency range of 20-100 Hz, the experiments with $\Phi = 0.55$ exhibit a dynamic gain of at least 3 to 5 dB lower than that observed for the other

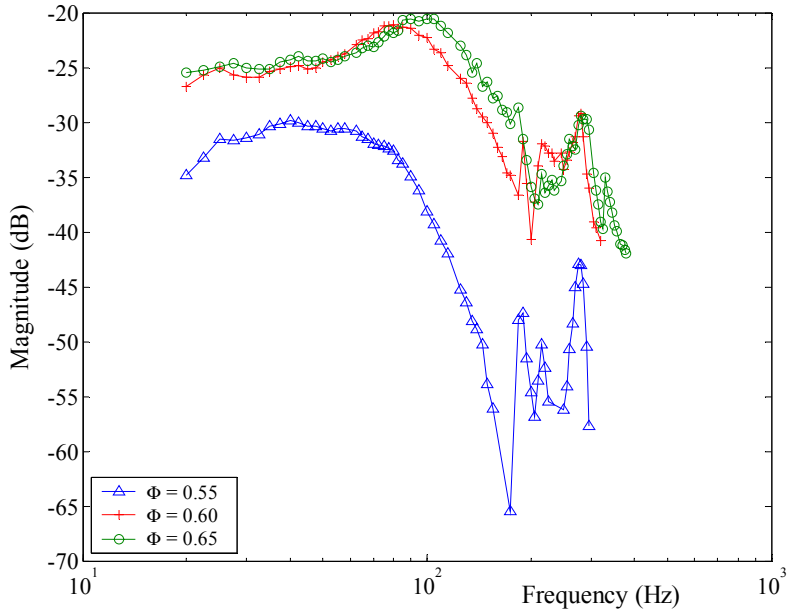

Figure 10.1: FRF (magnitude) for $Q_{Air} = 15$ scfm, $S = 0.79$ under fully premixed conditions

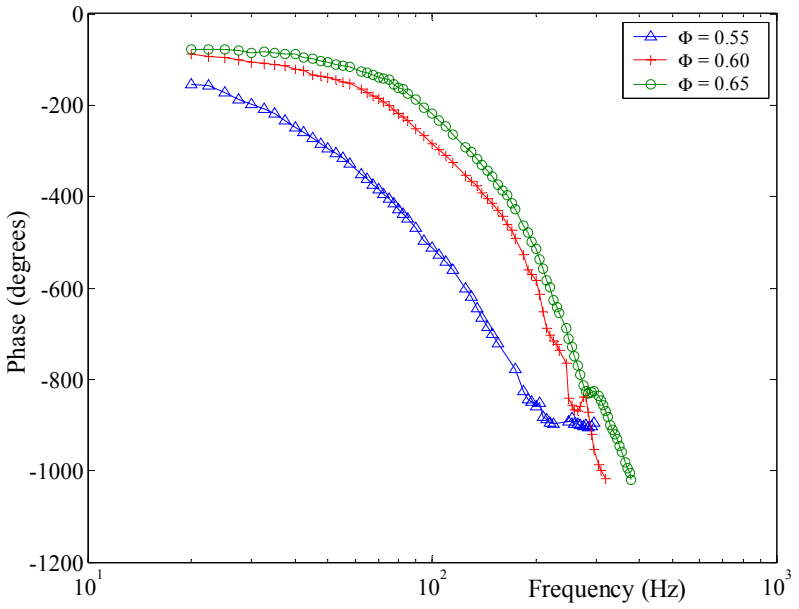

Figure 10.2: FRF (phase) for $Q_{Air} = 15$ scfm, $S = 0.79$ under fully premixed conditions

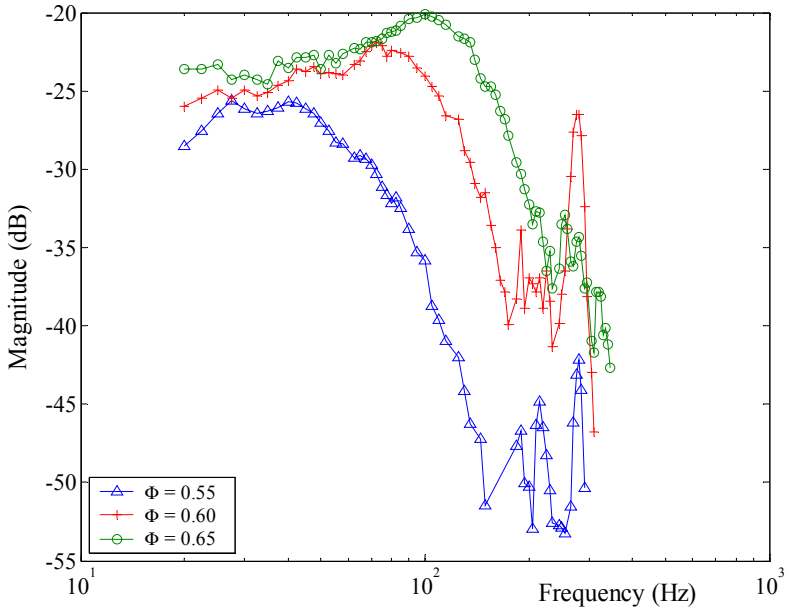

Figure 10.3: FRF (magnitude) for $Q_{Air} = 15$ scfm, $S = 1.19$ under fully premixed conditions

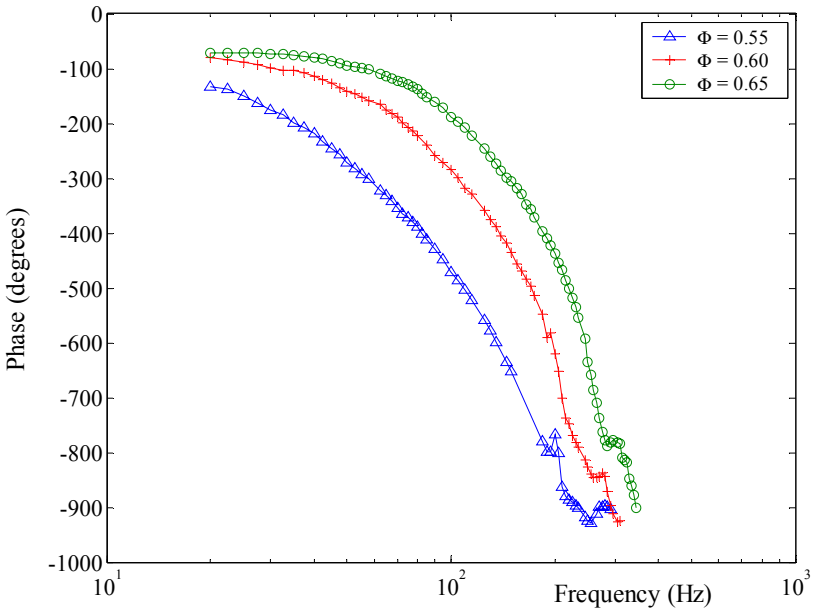

Figure 10.4: FRF (phase) for $Q_{Air} = 15$ scfm, $S = 1.19$ under fully premixed conditions

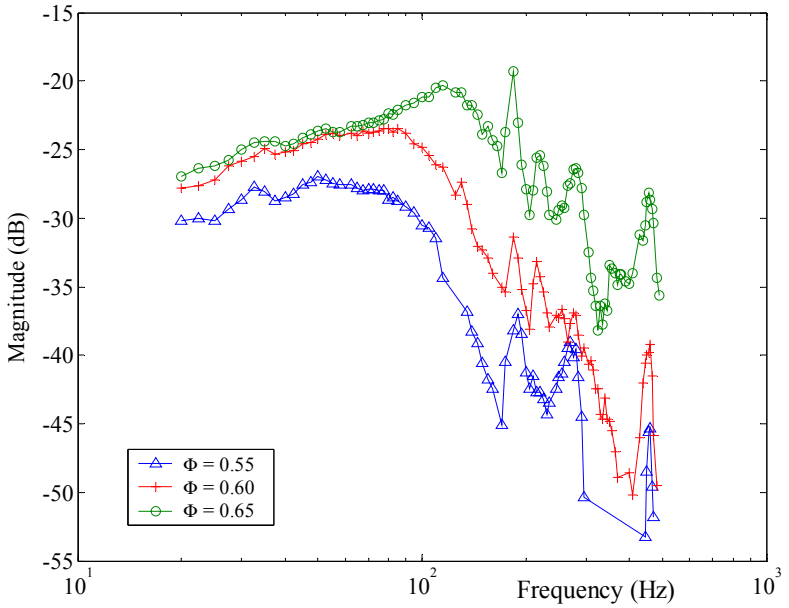

Figure 10.5: FRF (magnitude) for $Q_{Air} = 20$ scfm, $S = 0.79$ under fully premixed conditions

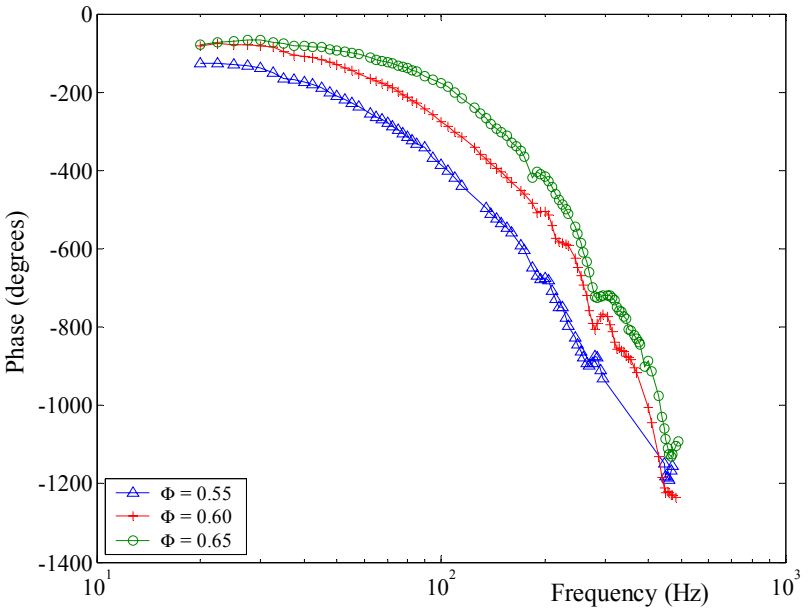

Figure 10.6: FRF (phase) for $Q_{Air} = 20$ scfm, $S = 0.79$ under fully premixed conditions

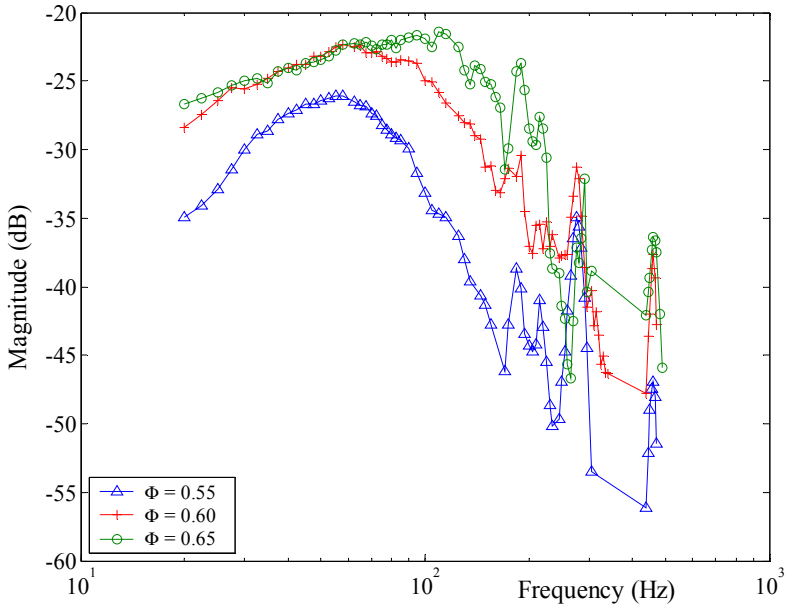

Figure 10.7: FRF (magnitude) for $Q_{Air} = 20$ scfm, $S = 1.19$ under fully premixed conditions

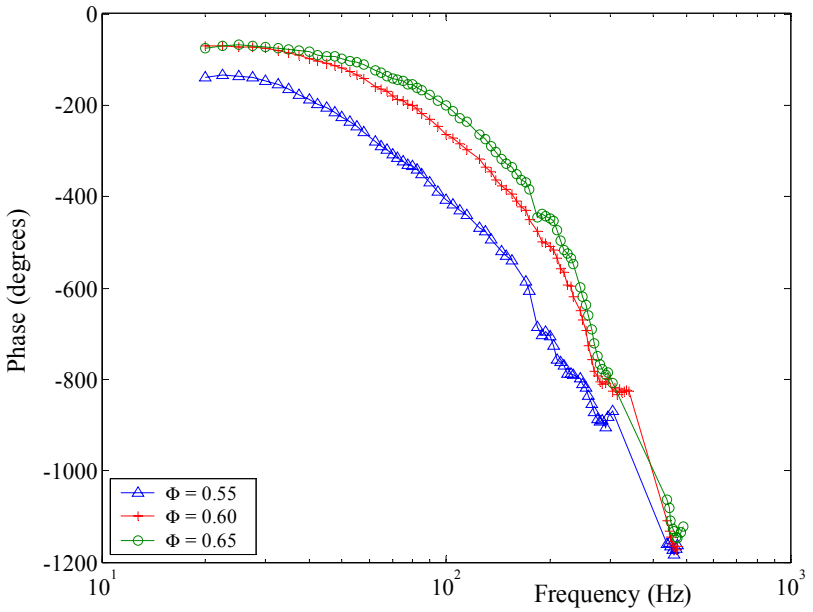

Figure 10.8: FRF (phase) for $Q_{Air} = 20$ scfm, $S = 1.19$ under fully premixed conditions

two equivalence ratios studied, while the conditions with $\Phi = 0.6$ and $\Phi = 0.65$ generally exhibit a similar dynamic gain. Beyond 100 Hz, the dynamic response for $\Phi = 0.60$ exhibits a lower dynamic gain when compared to the response for $\Phi = 0.65$, primarily due to the fact that results for $\Phi = 0.65$ have a broader bandwidth. All the magnitude plots show a distinct peak at 270 Hz, which results in a local increase in the dynamic gain of 4 to 15 dB. Some of the data also demonstrates smaller peaks at 190 Hz. For $Q_{Air} = 20$ scfm, data beyond 380 Hz also shows a distinct peak at 460 Hz. When compared to the Figure 9.3 of Chapter 9, these frequencies of 190, 270, and 460 correspond to the longitudinal acoustic modes of the rig. The implication of their distinct appearance is discussed in Section 10.6. However, lowering the swirl number seems to slightly dampen the response at these frequencies. All the magnitude plots show that the dynamic response tends to maintain its bandwidth (steady dynamic gain) between 170 Hz and 270 Hz.

Figures 10.2, 10.4, 10.6 and 10.8 detail the phase of the FRF. These plots show that the phase at 20 Hz for $\Phi = 0.55$ is always lower than those at $\Phi = 0.6$ and $\Phi = 0.65$ by about 50 degrees. At any particular frequency, the difference in phase between $\Phi = 0.55$ and the other two equivalence ratios is quite significant, but the phase at conditions with $\Phi = 0.65$ is almost the same as that seen with $\Phi = 0.6$ at all the frequencies. At the higher end of the frequency spectrum studied, the phase for all the three equivalence ratios almost merge together. Over the range of 20 to 400 Hz, all the experimental data exhibits a phase drop of about 900 degrees, which is indicative of the high order of the dynamics involved.

From the above observations, it can be concluded that within the frequency range of 100-400 Hz, small changes in Φ have a measurable impact on the dynamics of the combustion process. For the frequency range of 20-100 Hz, small changes in Φ around the lower equivalence ratios such as $\Phi = 0.55$, significantly effect the dynamic response of the flame, but at operating conditions with $\Phi \geq 0.6$, the effect of changes in Φ on the flame dynamics can be considered to be negligible. Therefore, well tuned stable combustors operating under ultra lean conditions are likely to exhibit thermo-acoustic instabilities, for small changes in the overall Φ.

To evaluate the influence of total air flow rates and swirl numbers on the FRF, the experimental data at $\Phi = 0.55$ and $\Phi = 0.65$ are plotted for all the flow rates and the swirl numbers in Figure 10.9 through Figure 10.12. Figure 10.9 and Figure 10.11 show the magnitude of the FRF for $\Phi = 0.55$ and $\Phi = 0.65$ respectively, while Figure 10.10 and Figure 10.12 show the phase of the FRF for $\Phi = 0.55$ and $\Phi = 0.65$ respectively. Both the magnitude and the phase plots show little effect of swirl number variation, but demonstrate a broadening of the bandwidth with increase in Q_{Air}. This phenomenon is more pronounced for $\Phi = 0.55$ than for $\Phi = 0.65$. a similar effect was seen earlier with respect to the increase in Φ. Thus, upon correlating this phenomenon to the conclusions of the laminar flat flame, it can be deduced that the broadening in the bandwidth is controlled by the reaction rate and the thermal interaction between the flame front and its surroundings. The response for conditions at $\Phi = 0.55$ show some increase in the dynamic gain for an increase in swirl number, within the frequency range of 20-100 Hz, but this effect diminishes with increase in Φ, as is seen from Figure 10.11.

10.3 Experimental Results for Partially Premixed Conditions

Experiments were conducted for the same range of overall Φ, Q_{Air} and S, that were studied under fully premixed conditions. Equality of the conditions was chosen primarily to be able to compare between the two types of experiments. The partially premixed conditions were generated by injecting fuel into the swirling air stream, in a plane that is 150 mm upstream of the inlet of the quarl. This generated a mixing condition analogous to jets in cross flow. Determination of the effects of variation in the unmixedness of the reactant stream were not conducted and left for future studies.

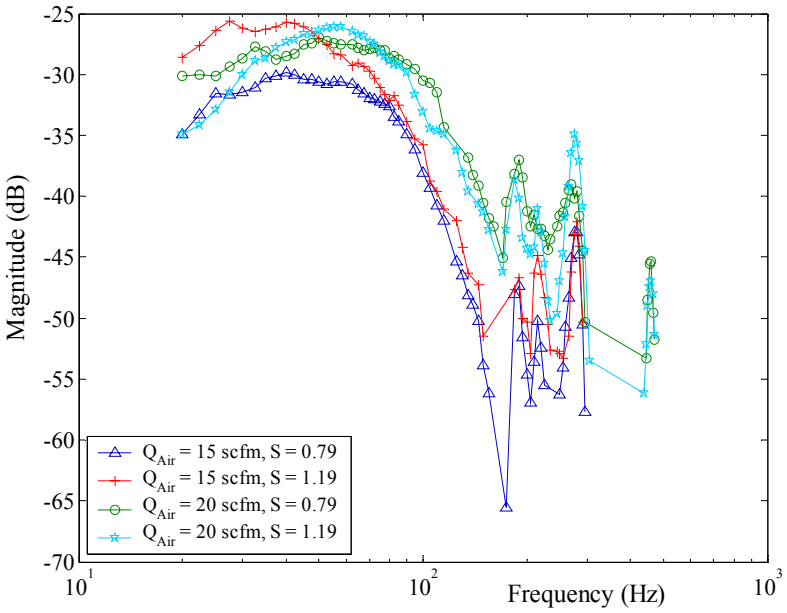

Figure 10.9: FRF (magnitude) for $\Phi = 0.55$ under fully premixed conditions

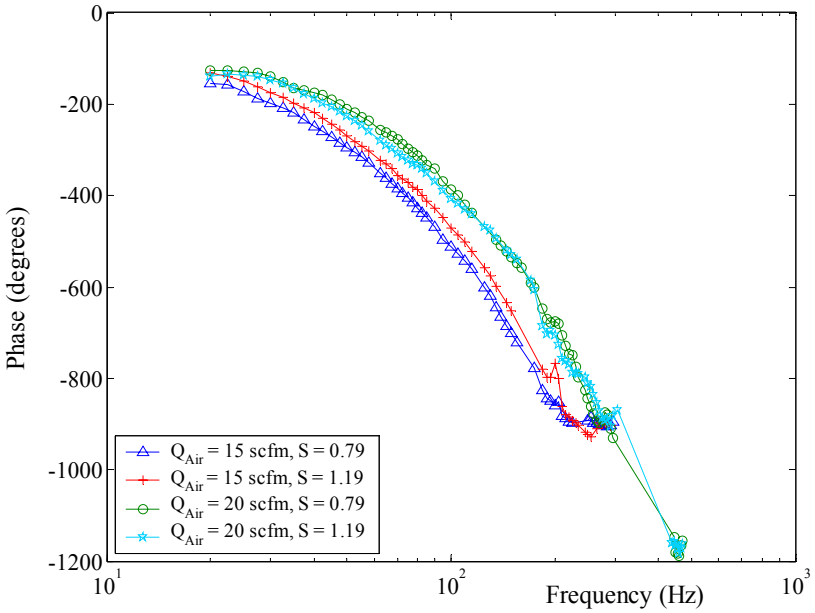

Figure 10.10: FRF (phase) for $\Phi = 0.55$ under fully premixed conditions

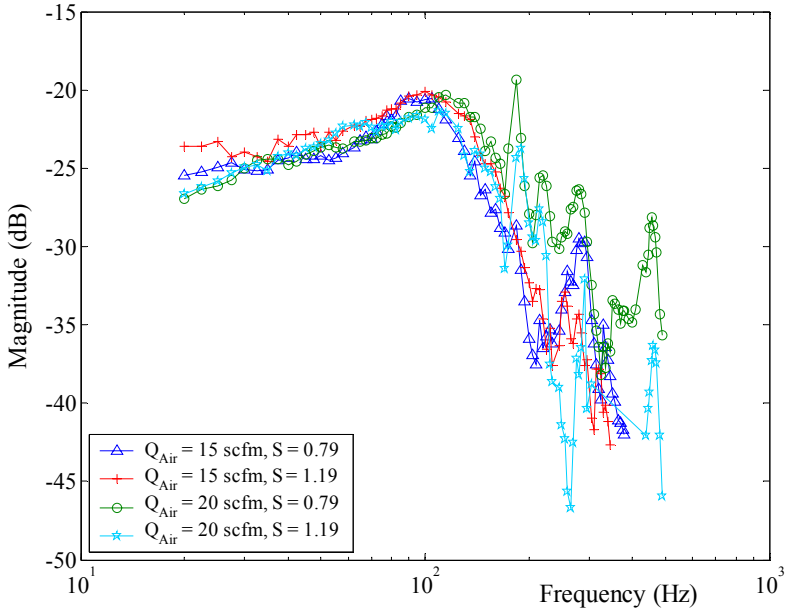

Figure 10.11: FRF (magnitude) for $\Phi = 0.65$ under fully premixed conditions

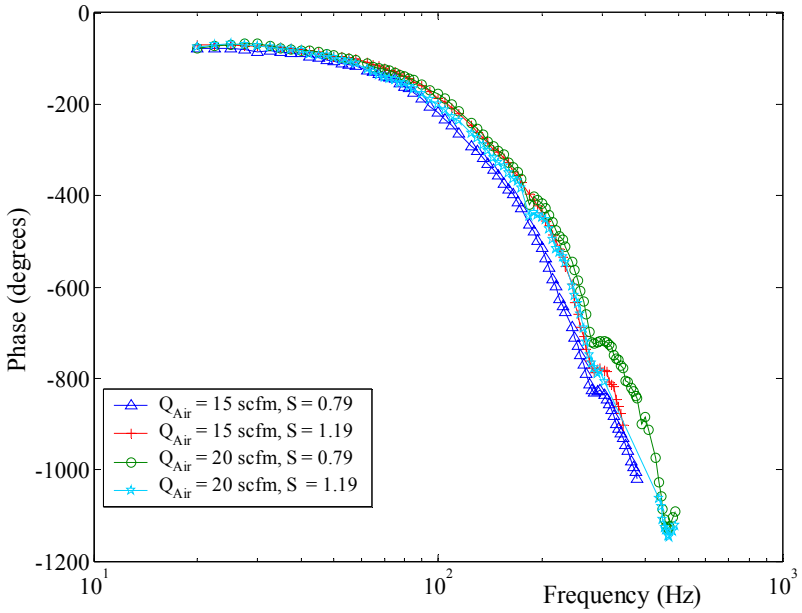

Figure 10.12: FRF (phase) for $\Phi = 0.65$ under fully premixed conditions

10.3.1 Interpretation of the Results

Figure 10.13 through Figure 10.20 show the magnitude and the phase of the FRF between the OH^* chemiluminescence signal and u' for the two flow rates and the two swirl numbers. For $Q_{Air} = 15$ scfm, data was taken between 20 and 380 Hz, while for $Q_{Air} = 20$ scfm, data was collected between 20 and 490 Hz. Figures 10.13, 10.15, 10.17 and 10.19 detail the magnitude of the FRF. These figures show that the dynamics of partially premixed flames exhibit a rich spectra, that attempts to maintain its bandwidth over the entire range of frequency studied. The response shows the presence of zero at low frequencies. For $S = 0.79$, the zero location shifts to lower frequencies, while for $S = 1.19$, the frequency of the zero is not effected by the change in Φ, but the magnitude of the drop in the dynamic gain at the location of the zero is reduced as Φ is increased. Further, data for $S = 1.19$ shows the presence of a smaller number of zeros when compared to the data for $S = 0.79$, thus giving its FRF a more orderly appearance than that for $S = 0.79$. These differences between $S = 0.79$ and $S = 1.19$ are probably due to the distribution of the concentration of the reactants across the cross-section of the flow. From the presented experimental results, it is noted that the peaks at 190, 270 and 460 Hz, the acoustic modes of the combustor, are prominent and well defined. Change in Φ seems to have little effect on the increase in the dynamic gain at these acoustic modes.

Figure 10.14, 10.16, 10.18 and 10.20 detail the phase of the FRF. These plots show that for $S = 0.79$, the phase for $\Phi = 0.55$ behaves very differently as compared to the phase for $\Phi = 0.6$ and $\Phi = 0.65$. However, at $S = 1.19$, there is little difference in the phase between the three equivalence ratios.

To evaluate the influence of Q_{Air} on the FRF, the experimental data for $\Phi = 0.55$ and $\Phi = 0.65$, categorized by the swirl number are plotted in Figure 10.21 through Figure 10.28. Figures 10.21, 10.25, 10.25 and 10.27 detail the magnitude of the FRF, while the Figures 10.22, 10.24, 10.26 and 10.28 detail the phase of the FRF. The phase plots of the FRF show very little influence of Q_{Air}, except for the region where the low frequency zero resides. The

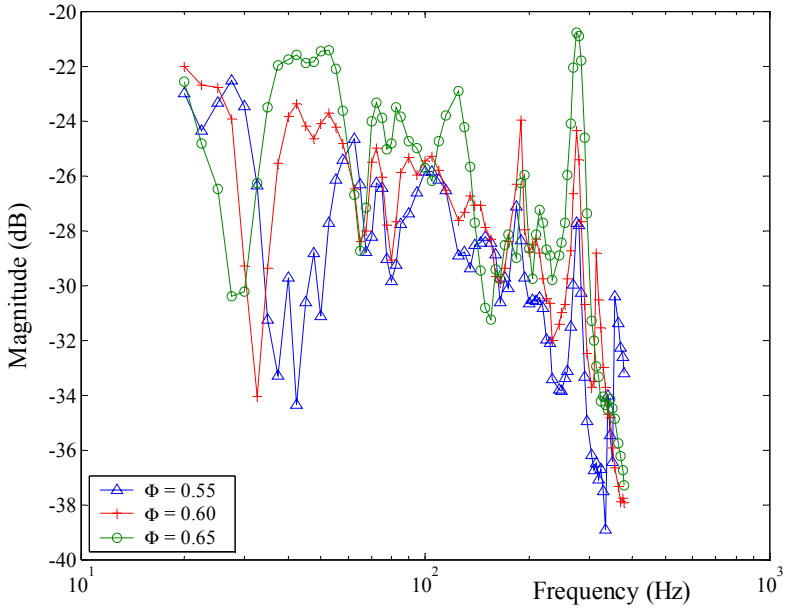

Figure 10.13: FRF (magnitude) for $Q_{Air} = 15$ scfm, $S = 0.79$ under partially premixed conditions

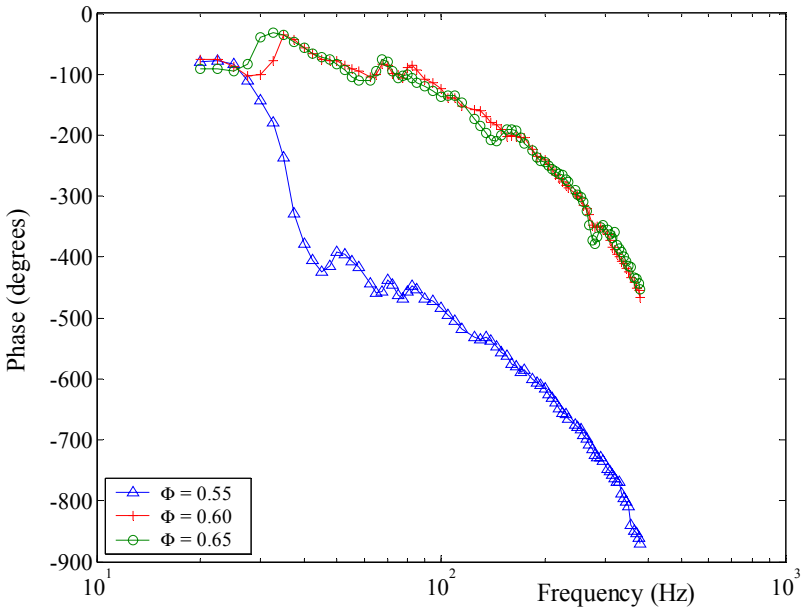

Figure 10.14: FRF (phase) for $Q_{Air} = 15$ scfm, $S = 0.79$ under partially premixed conditions

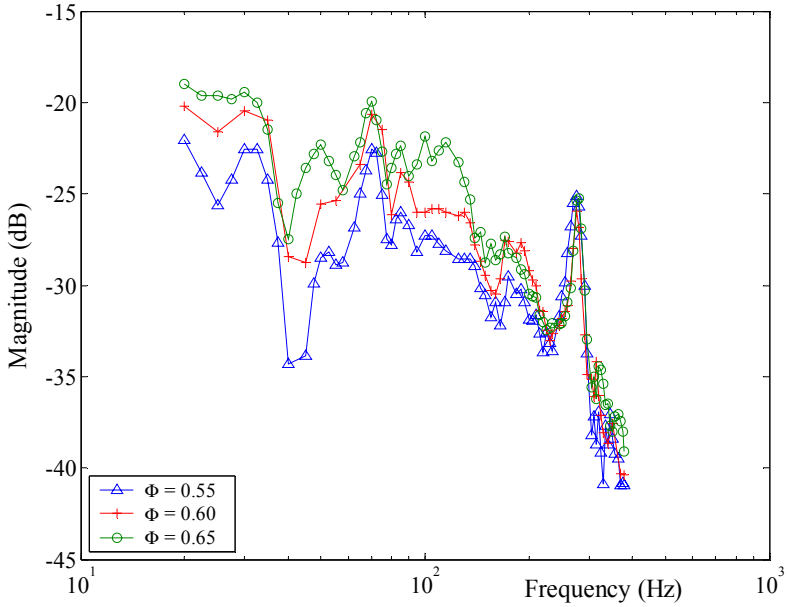

Figure 10.15: FRF (magnitude) for $Q_{Air} = 15$ scfm, $S = 1.19$ under partially premixed conditions

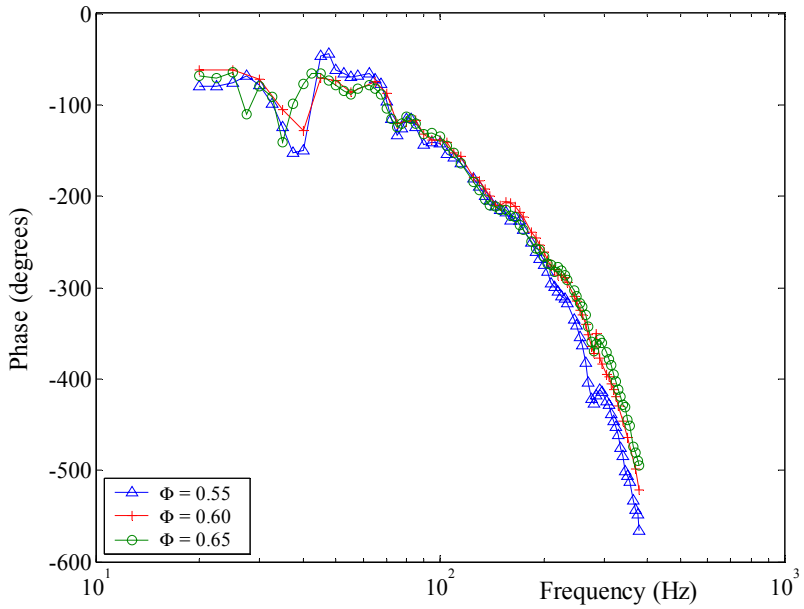

Figure 10.16: FRF (phase) for $Q_{Air} = 15$ scfm, $S = 1.19$ under partially premixed conditions

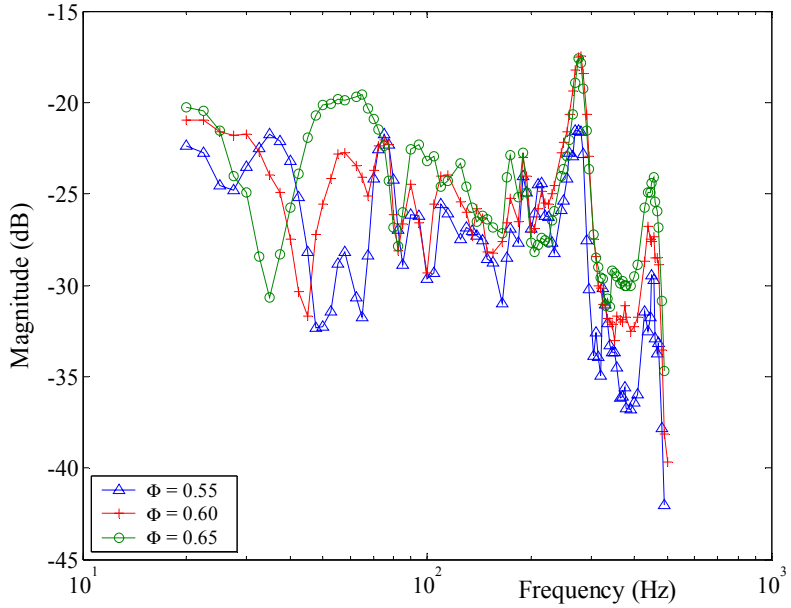

Figure 10.17: FRF (magnitude) for $Q_{Air} = 20$ scfm, $S = 0.79$ under partially premixed conditions

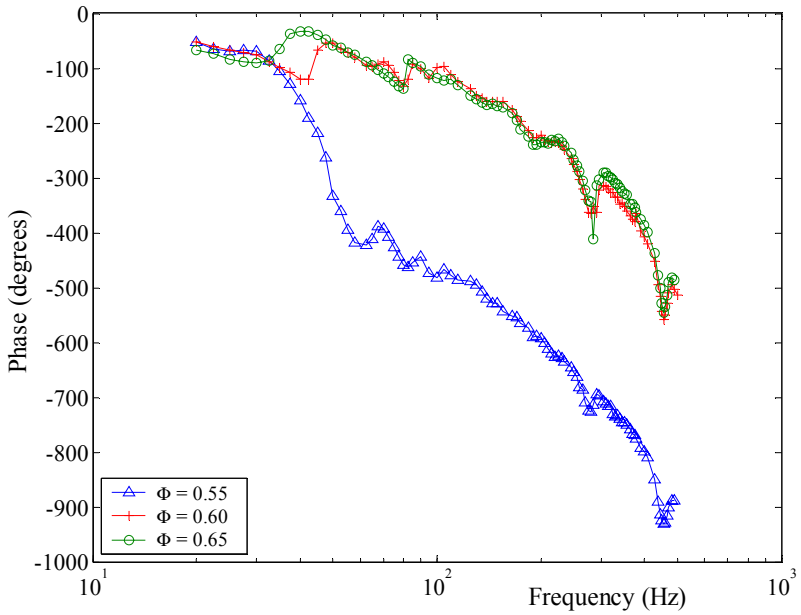

Figure 10.18: FRF (phase) for $Q_{Air} = 20$ scfm, $S = 0.79$ under partially premixed conditions

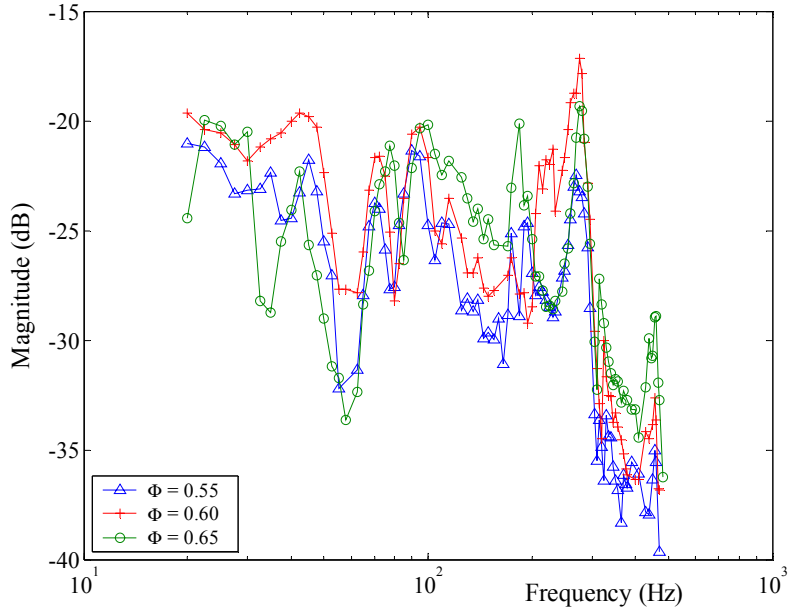

Figure 10.19: FRF (magnitude) for $Q_{Air} = 20$ scfm, $S = 1.19$ under partially premixed conditions

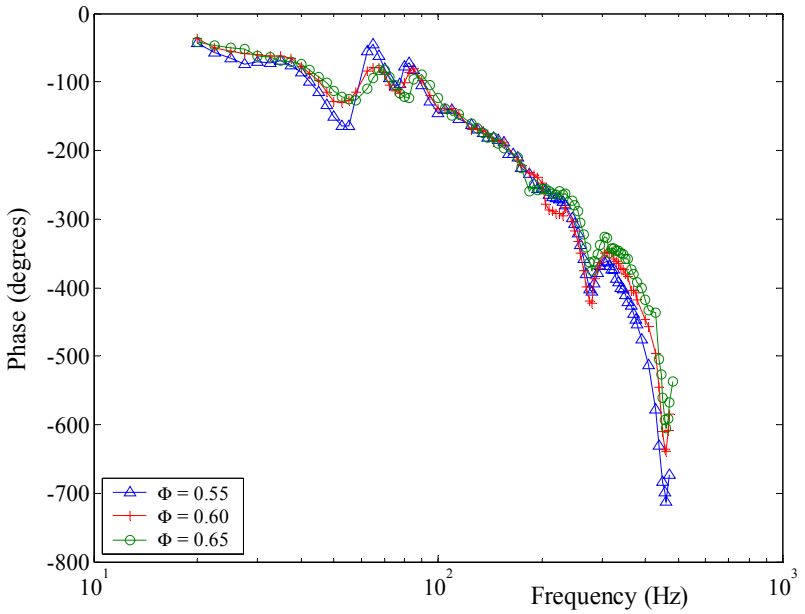

Figure 10.20: FRF (phase) for $Q_{Air} = 20$ scfm, $S = 1.19$ under partially premixed conditions

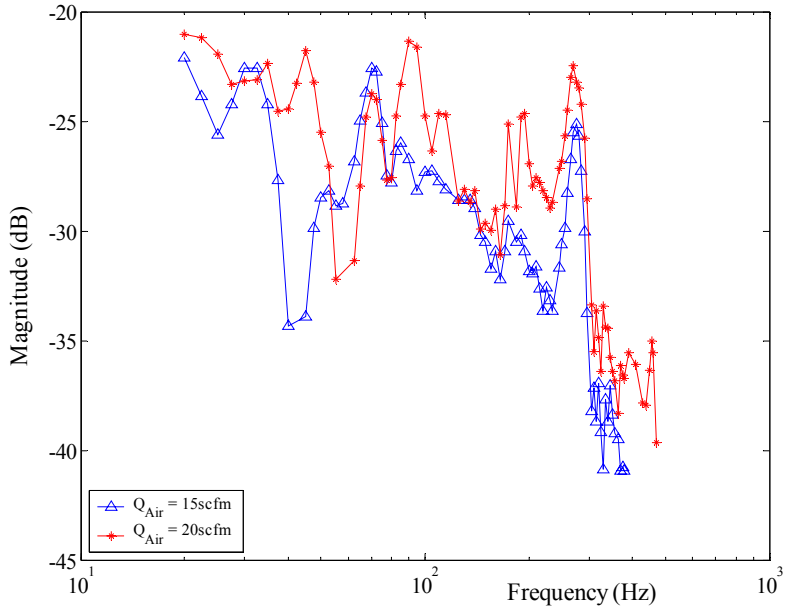

Figure 10.21: FRF (magnitude) for $S = 1.19$, $\Phi = 0.55$ under partially premixed conditions

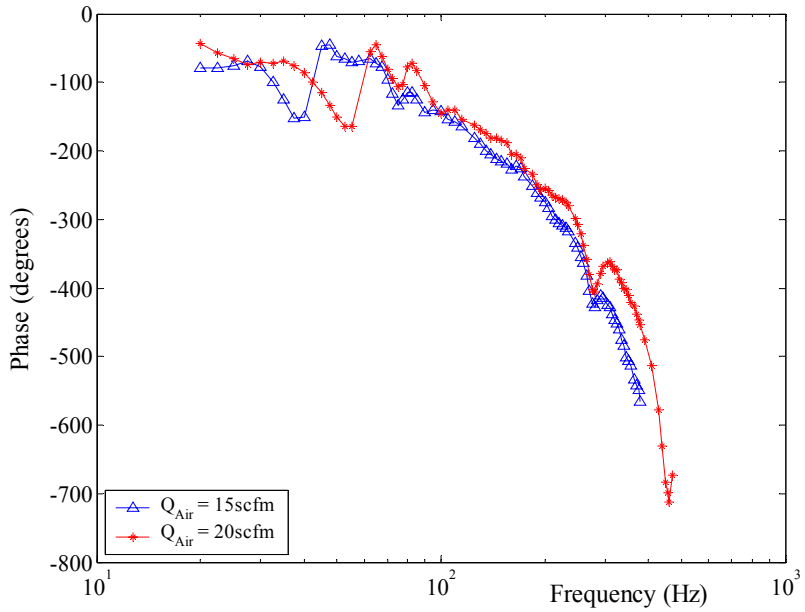

Figure 10.22: FRF (phase) for $S = 1.19$, $\Phi = 0.55$ under partially premixed conditions

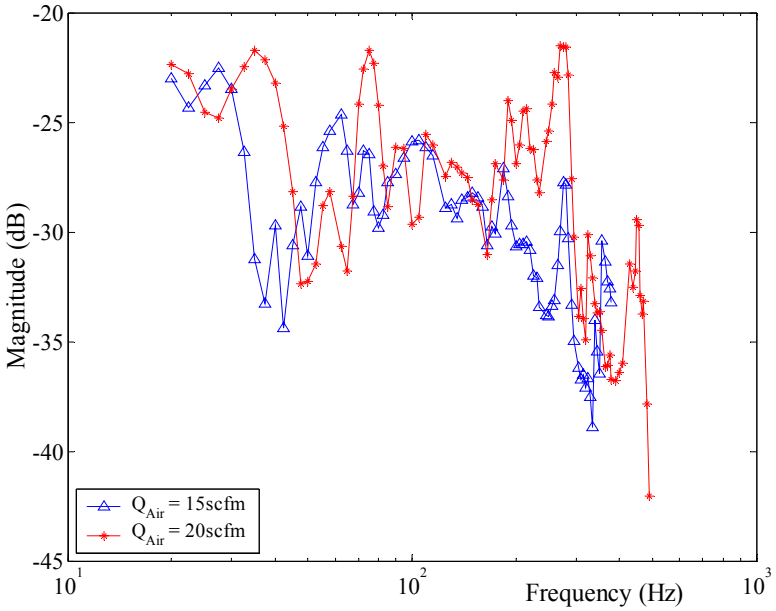

Figure 10.23: FRF (magnitude) for $S = 0.79$, $\Phi = 0.55$ under partially premixed conditions

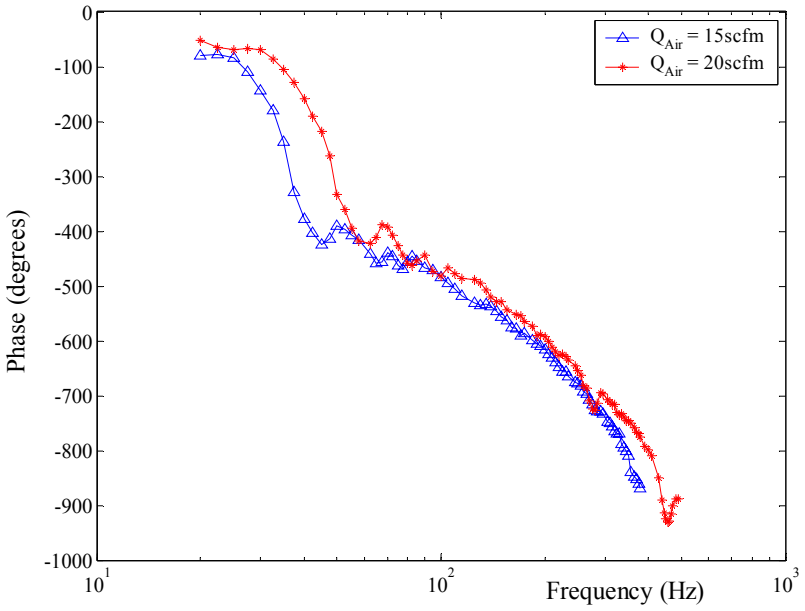

Figure 10.24: FRF (phase) for $S = 0.79$, $\Phi = 0.55$ under partially premixed conditions

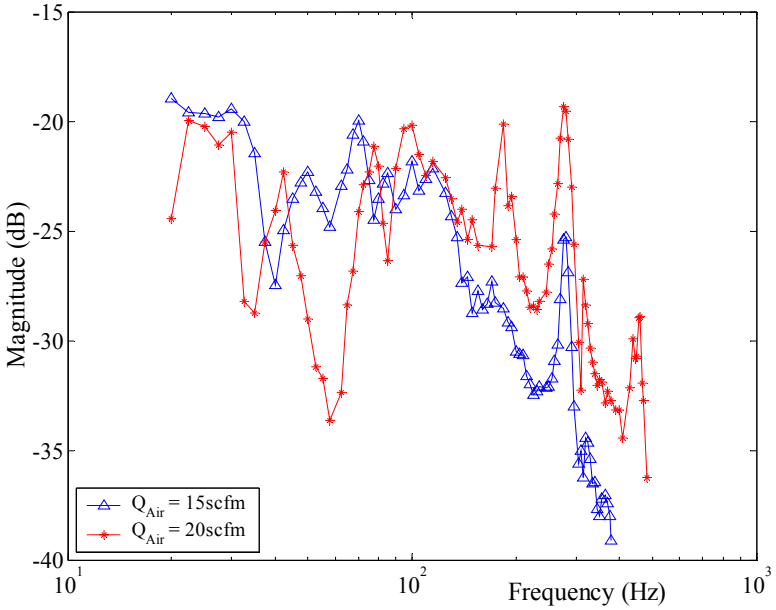

Figure 10.25: FRF (magnitude) for $S = 1.19$, $\Phi = 0.65$ under partially premixed conditions

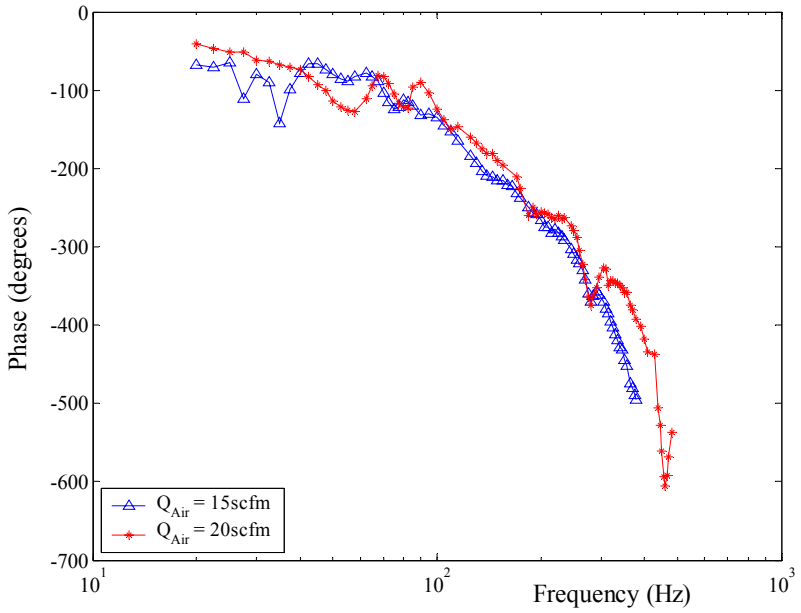

Figure 10.26: FRF (phase) for $S = 1.19$, $\Phi = 0.65$ under partially premixed conditions

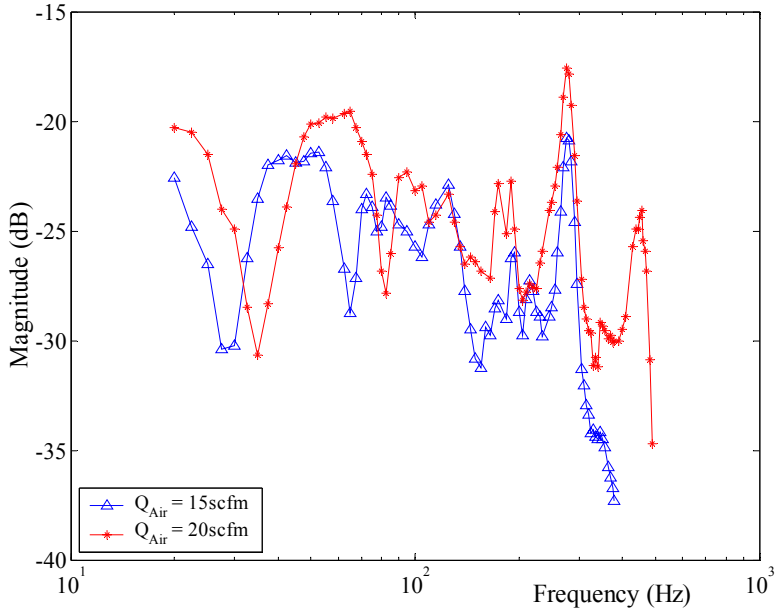

Figure 10.27: FRF (magnitude) for $S = 0.79$, $\Phi = 0.65$ under partially premixed conditions

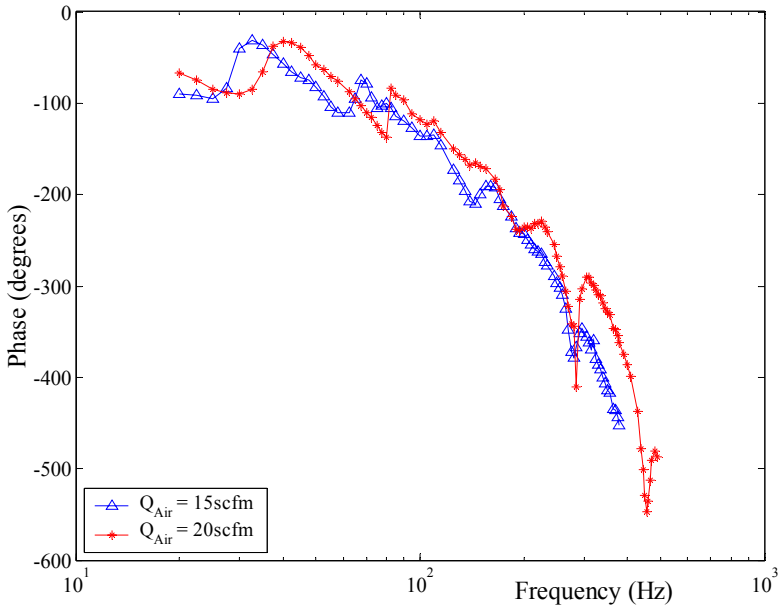

Figure 10.28: FRF (phase) for $S = 0.79$, $\Phi = 0.65$ under partially premixed conditions

magnitude plots also clearly indicate that an increase in the flow rate tends to increase the bandwidth of the response and also makes the peaks occurring at the acoustic modes of 270 Hz and 460 Hz more pronounced. The zero which occurs at a low frequency (between 30-60 Hz) shifts to a higher frequency with an increase in the flow rate.

Comparing the observation made for the influence of Q_{Air} with the effects of S and Φ on the presence of the low frequency zero, it is noted that each of these parameters exhibits a different effect on these low frequencies zeros. Q_{Air} and Φ move the zeros in the opposite directions on the frequency axis, while increasing S tends to diminish their presence. It should be noted that under fully premixed conditions, these zeros were not prominent in the data. All of the above observations indicate that the location of the zero and probably also its damping, is influenced by the local instantaneous species distribution across the cross-section of the flow, as it arrives at the flame front. Had the air flow been steady, the only variable involved would have been the species distribution across the cross-section of the flow (also termed as the unmixedness of the mixture). But as the acoustic pressure oscillates in the combustor, it not only generates Φ oscillations at the plane of the fuel injection, but also influences the mixing process. Furthermore, it is known that the influence of Φ oscillations is dependent upon the local mean Φ [84]. As the mean Φ decreases, Φ oscillations have a stronger impact on the heat release. Thus, at every instant in the cycle, each small region of the flame front experiences a different species distribution and at any particular position, the flame front experiences an oscillatory species distribution in time. The net result, as seen from the dynamic plot is an integrated effect of all such local variations.

To gain further insight to the behavior of the partially premixed flames, it is recommended that a detailed study of the species distribution for various swirl numbers and for various fuel injection planes be conducted in the near future. Additionally, future research should concentrate on understanding and controlling the mixing process, and predicting its effect on the flame dynamics. These studies could have far reaching influences on the design of active combustion control systems that could accurately control the species distribution in the flow. The study will also help in designing algorithms for sub-harmonic controllers, as

it would be very essential to predict accurately the presence of the low frequency zeros, so that the controller can adjust its control frequency to be away from that of the zero, and not loose authority over the process.

10.4 Comparison of Fully and Partially Premixed Experiments

Figure 10.29 through Figure 10.36 show the FRF magnitude and the phase comparison of the fully and partially premixed experiments for the two swirl numbers and $\Phi = 0.55$ and $\Phi = 0.65$. Figures 10.29, 10.31, 10.33 and 10.35 show the magnitude of the FRF, while Figures 10.30, 10.32, 10.34 and 10.36 describe the phase of the FRF. For $\Phi = 0.55$, in the frequency range of 200-400 Hz, the magnitude plots indicate that the dynamic gain of the totally premixed flames is almost an order of magnitude lower than that of the partially premixed conditions. This primarily occurs due to the fact that partially premixed flames exhibit a broad bandwidth of response that extends right up to 400 Hz, while the fully premixed flames show a low pass filtering response with the corner frequency around 100 Hz. When comparing the magnitude of the fully and the partially premixed conditions at $\Phi = 0.65$, it is noted that the difference in the dynamic gain in the frequency range of 20 to 400 Hz has reduced considerably. Yet, at the acoustic modes, the magnitude of the peaks for the fully premixed conditions is still around 10 dB lower than that for partially premixed conditions. The phase plots for all the conditions compared show that the phase for partially premixed cases is quite different than that for fully premixed conditions. Except for $\Phi = 0.55$ and $S = 0.79$, the drop in phase for fully premixed condition in the frequency range of 20-400 Hz, is 400 to 650 degrees greater than the drop in phase for partially premixed conditions. Thus, situations can arise where this difference in phase (even after wrapping the phase between 0 and 360 degrees) is greater than the stability margin of the combustor.

The above discussion indicates that the phase is quite sensitive to the combination of Φ oscillations and to the variations in the species concentration across the cross-section of the

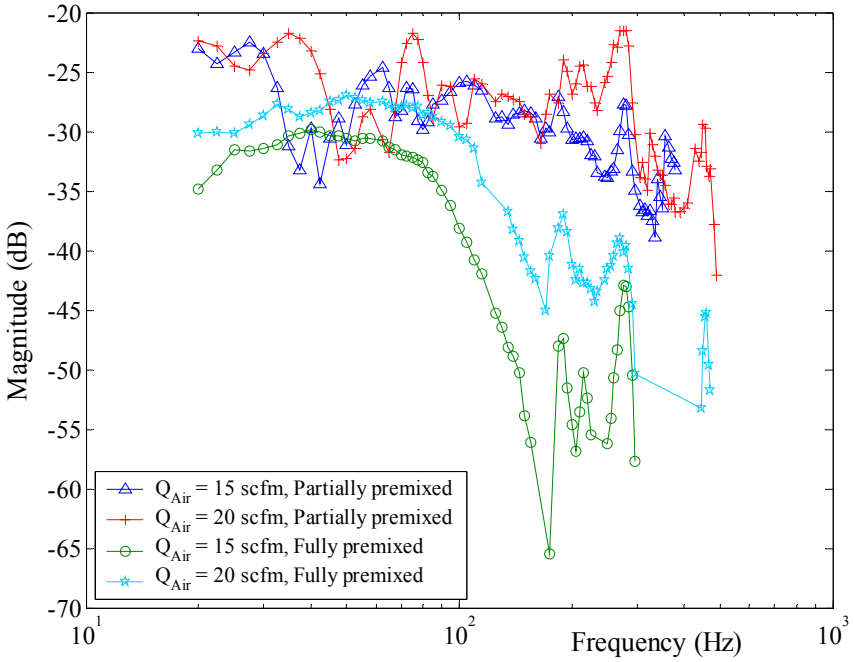

Figure 10.29: FRF (magnitude) for $\Phi = 0.55$, $S = 0.79$

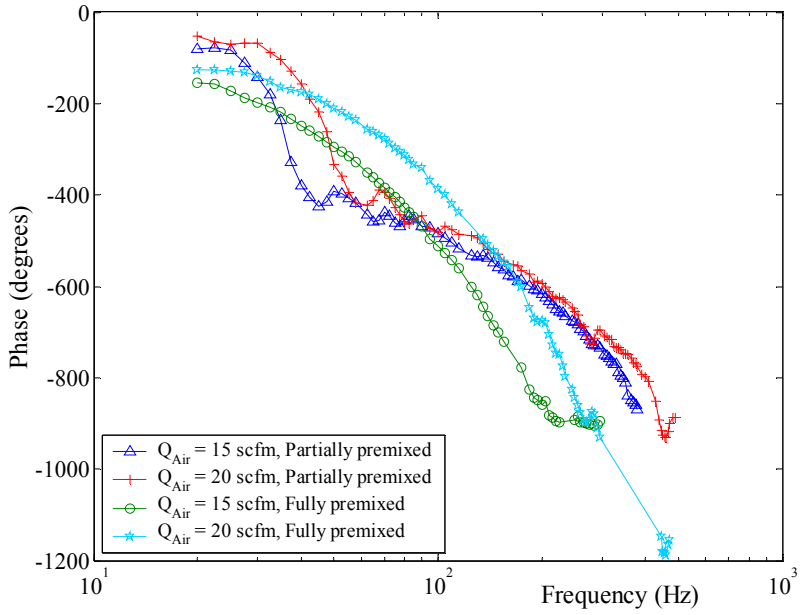

Figure 10.30: FRF (phase) for $\Phi = 0.55$, $S = 0.79$

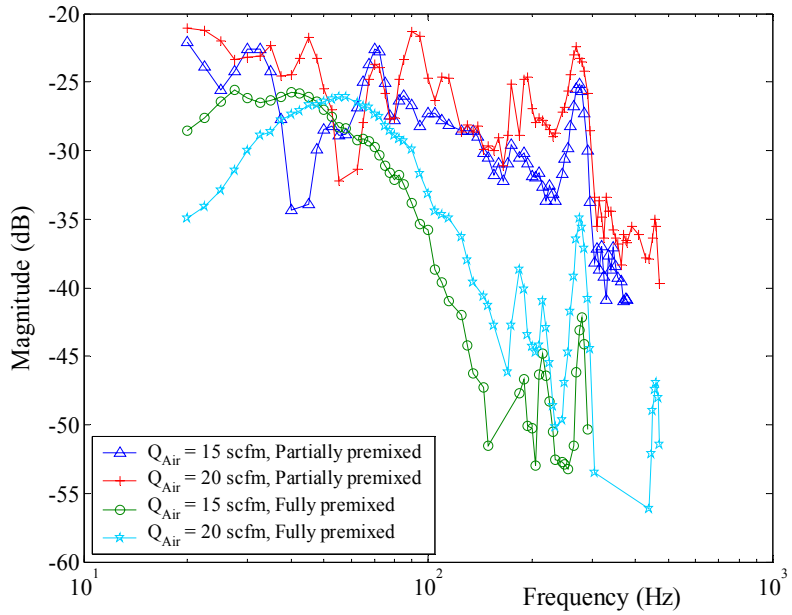

Figure 10.31: FRF (magnitude) for $\Phi = 0.55$, $S = 1.19$

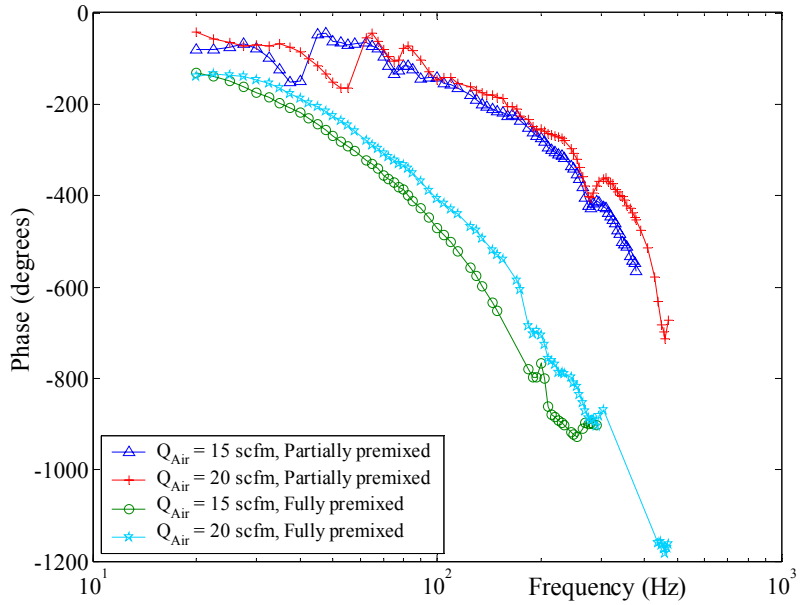

Figure 10.32: FRF (phase) for $\Phi = 0.55$, $S = 1.19$

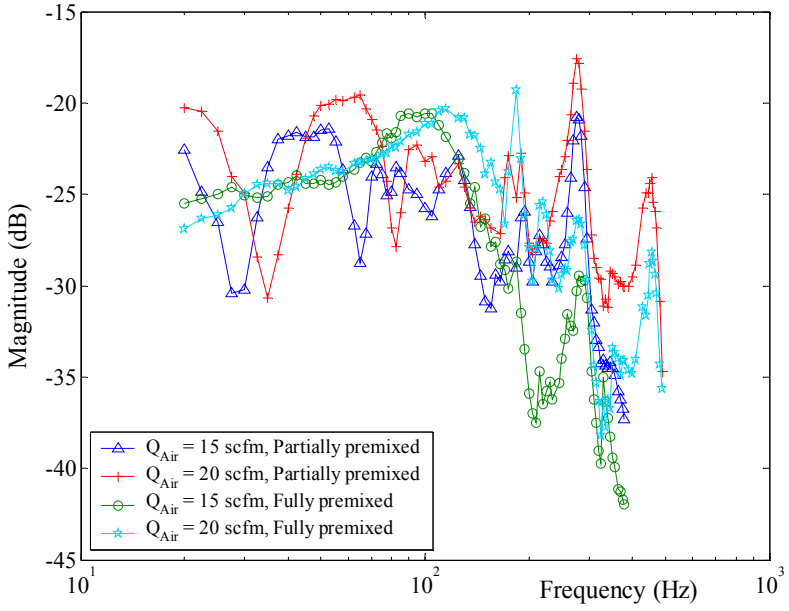

Figure 10.33: FRF (magnitude) for $\Phi = 0.65$, $S = 0.79$

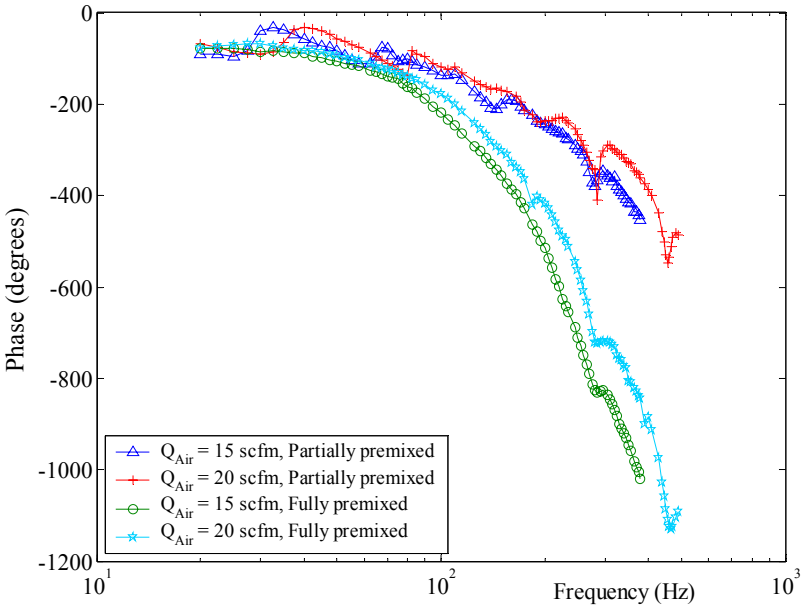

Figure 10.34: FRF (phase) for $\Phi = 0.65$, $S = 0.79$

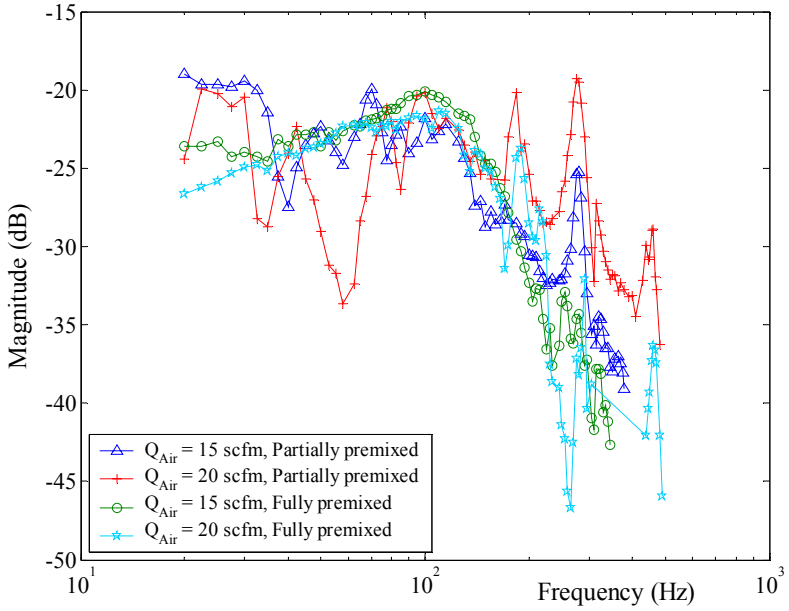

Figure 10.35: FRF (magnitude) for $\Phi = 0.65$, $S = 1.19$

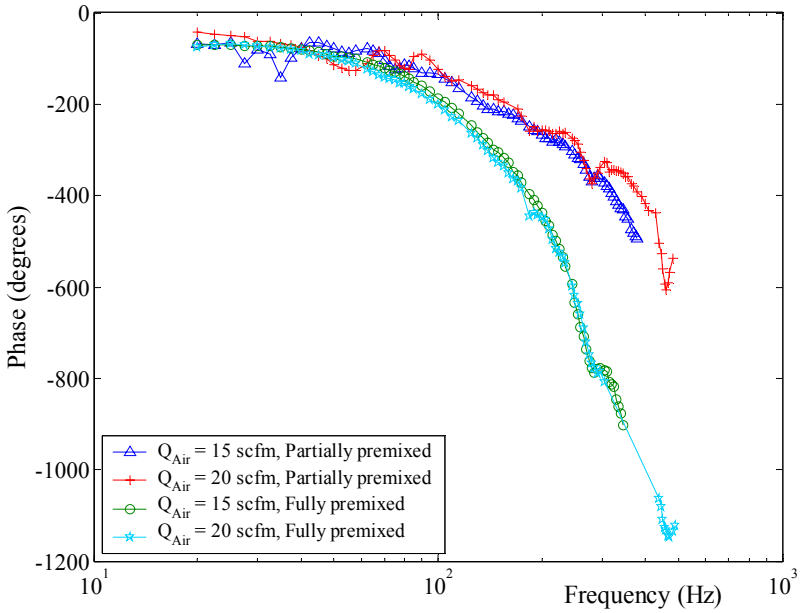

Figure 10.36: FRF (phase) for $\Phi = 0.65$, $S = 1.19$

flow. Furthermore, combustors with fully premixed flames have a higher probability of being thermo-acoustically stable than those with partially premixed flames, purely by the virtue of having a lower dynamic gain. Earlier research efforts by Flores et al. [68] and Wang et al. [85] have shown an increase in NO_x emissions with increase in the unmixedness of the reactant mixture. Thus, to achieve lower pollutant levels and to prevent the occurrence of thermo-acoustic instabilities, active control methodology must be primarily targeted towards minimizing both spatial and temporal variations in Φ. The author expects that such control methodologies would invariably include active control of the mixing process upstream of the flames. Detailed and systematic study, both experimental and computational, on the effects of variation in the unmixedness of the reacting mixture are required to enhance the predictability of thermo-acoustic instability and also to verify and build on the hypothesis presented here.

10.5 Reduced Order Dynamic Models

An attempt was made to model the experimental data so that a systems level reduced order model could be developed to predict the dynamics of swirl stabilized turbulent flames. However, due to the complex nature of the dynamics exhibited, there was very little success in developing such models. The author was unable to obtain reasonable models for the partially premixed experiments. However, there was a limited success in developing models for the fully premixed cases. The fully premixed conditions were modeled between the frequency range of 20 and 190 Hz leaving out the peaks at the acoustic modes, because as discussed in Section 10.6, their presence is due to a phenomenon not measured and accounted in this study.

The developed models are shown in Figure 10.37 through Figure 10.44 with their respective data. All the models exhibit an 8^{th} order response. The magnitude of the models match their respective data sets quite well for all the conditions studied, but a reasonable phase match is achieved only for conditions with $\Phi = 0.55$. The phase predicted by the models for

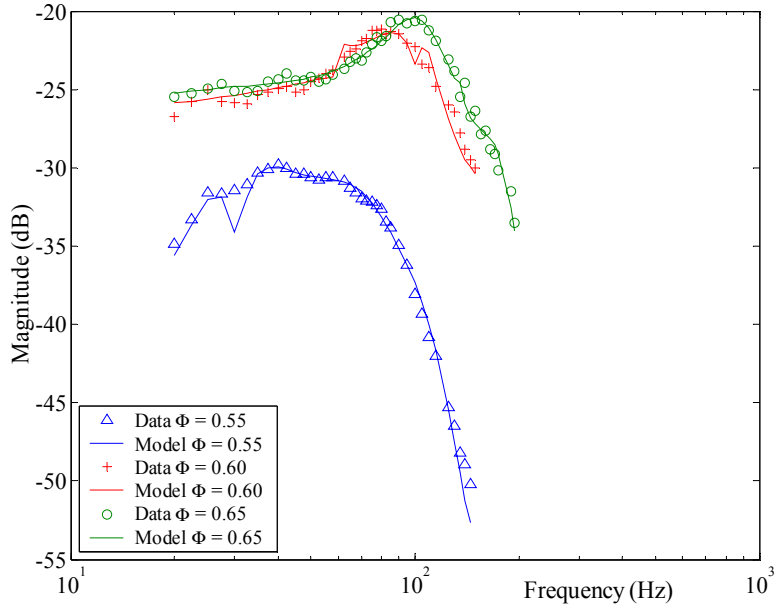

Figure 10.37: FRF (magnitude) for $Q_{Air} = 15$ scfm, $S = 0.79$ under fully premixed conditions

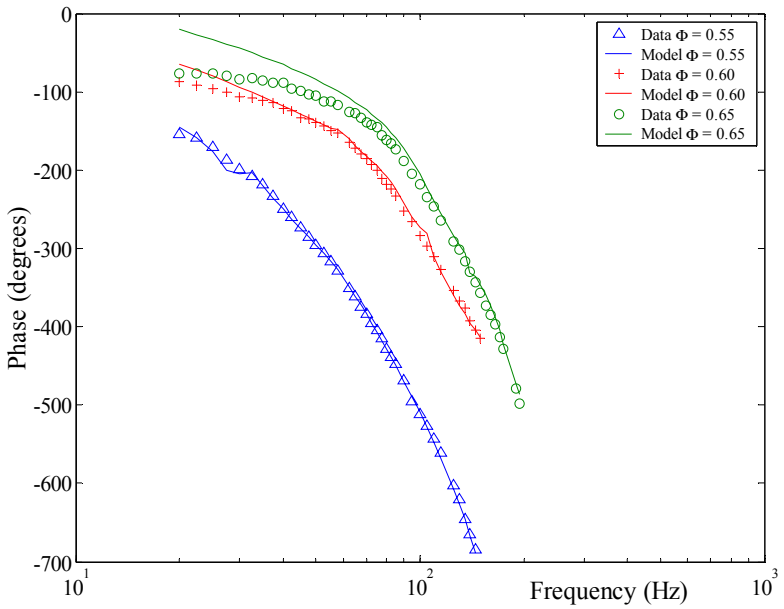

Figure 10.38: FRF (phase) for $Q_{Air} = 15$ scfm, $S = 0.79$ under fully premixed conditions

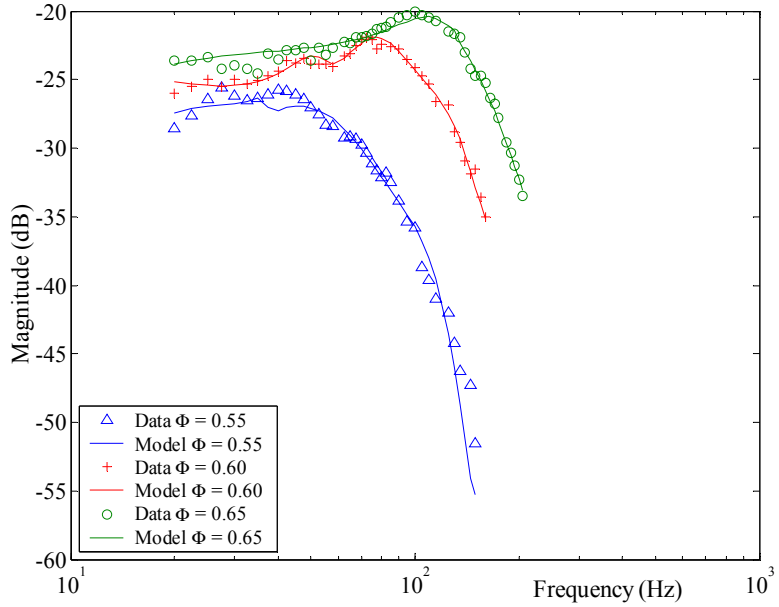

Figure 10.39: FRF (magnitude) for $Q_{Air} = 15$ scfm, $S = 1.19$ under fully premixed conditions

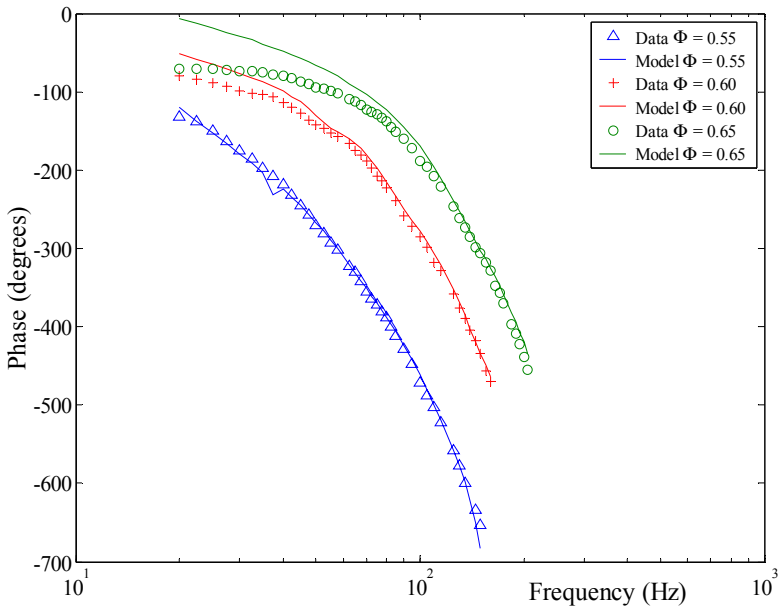

Figure 10.40: FRF (phase) for $Q_{Air} = 15$ scfm, $S = 1.19$ under fully premixed conditions

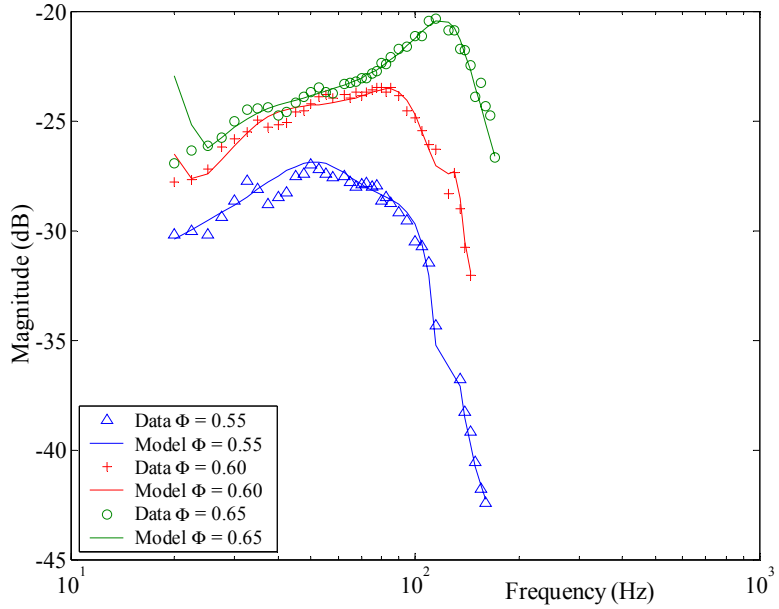

Figure 10.41: FRF (magnitude) for $Q_{Air} = 20$ scfm, $S = 0.79$ under fully premixed conditions

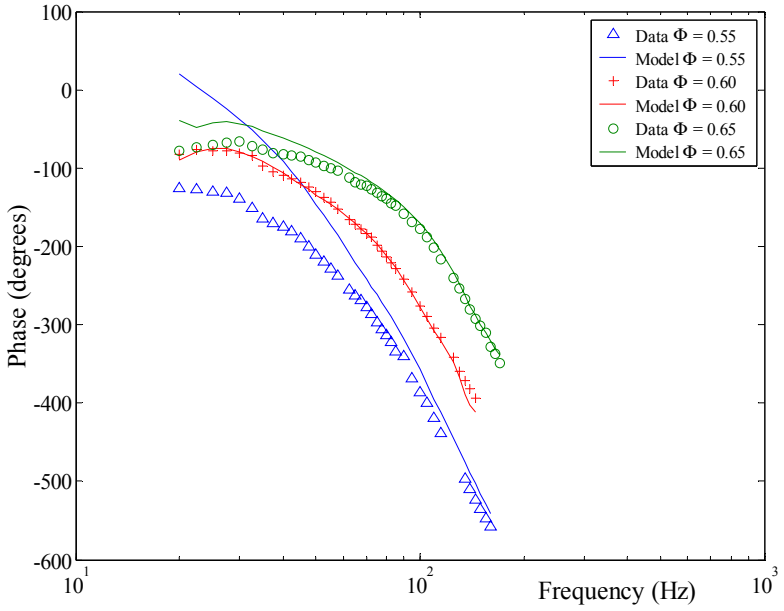

Figure 10.42: FRF (phase) for $Q_{Air} = 20$ scfm, $S = 0.79$ under fully premixed conditions

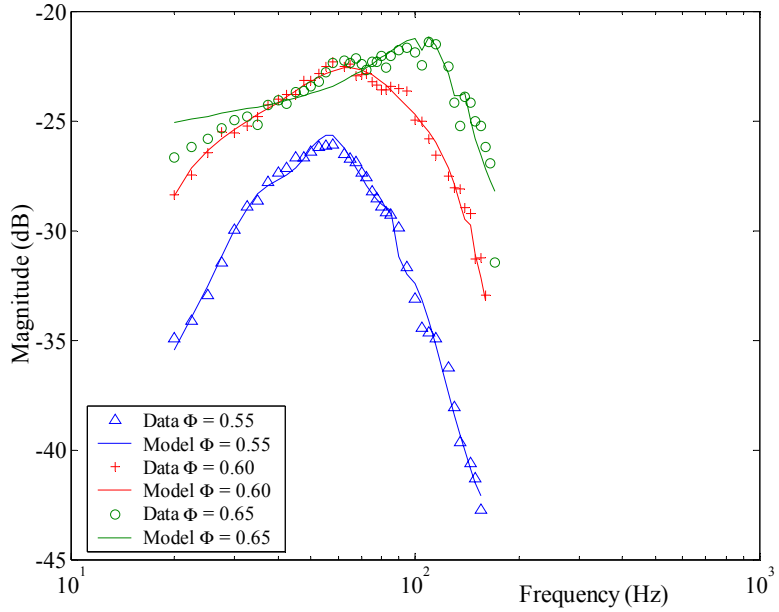

Figure 10.43: FRF (magnitude) for $Q_{Air} = 20$ scfm, $S = 1.19$ under fully premixed conditions

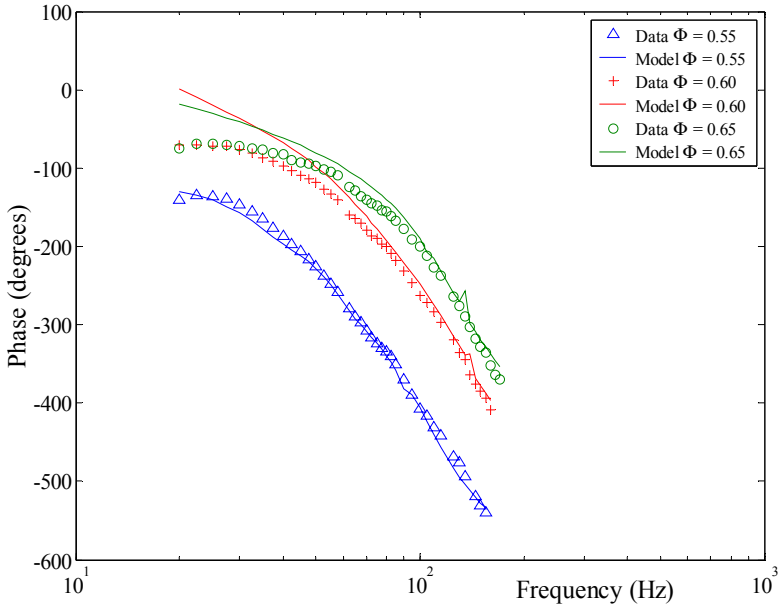

Figure 10.44: FRF (phase) for $Q_{Air} = 20$ scfm, $S = 1.19$ under fully premixed conditions

the conditions with $\Phi > 0.55$ deviate from the actual data in the low frequency range. The probable cause of this feature is the activation of some nonlinear response which effects the heat release output of the flame, but is not recorded by the measurement system used in these experiments. The models show that such a nonlinear response is quite sensitive to Φ, rather than Q_{Air} and S. The poles, zeros, and the gain values predicted by the model are detailed in Appendix D. However, due to the inaccuracies in the model described above and the limited amount of reasonable results, no attempt was made to correlate the predicted dynamics to the physical parameters.

10.6 Results of Reacting Flow Visualization

The dynamic results discussed in Section 10.2 and Section 10.3 showed that independent of the operating conditions, there was a sharp increase in the dynamic gain around the longitudinal acoustic modes of the combustor. To investigate this peculiar behavior, the power spectrum of both OH^* chemiluminescence and u' were plotted as a function of the frequency. Figure 10.45 compares the behavior of u' for the same constant excitation under

a. No flow velocity
b. $Q_{Air} = 15$ scfm, S = 1.2, cold flow
c. $Q_{Air} = 15$ scfm, S = 1.2, reacting flow

for a frequency range around the longitudinal acoustic mode at 275 Hz. The power spectrum for condition (b) closely follows the acoustic characteristics of the rig, thus eliminating the possibility of swirling flows causing a distortion in the reflected wave, and hence generating a nonlinear response. However, the condition (c) exhibits a very different trend in the u' magnitude which dips to -1.27 dBV at 280 Hz, instead of exhibiting a peak. Thus, there is a 4.8 dBV difference between conditions (b) and (c), indicating the presence of a nonlinear mechanism within the flame that distorts the reflected acoustic wave. This dip in the u' mag-

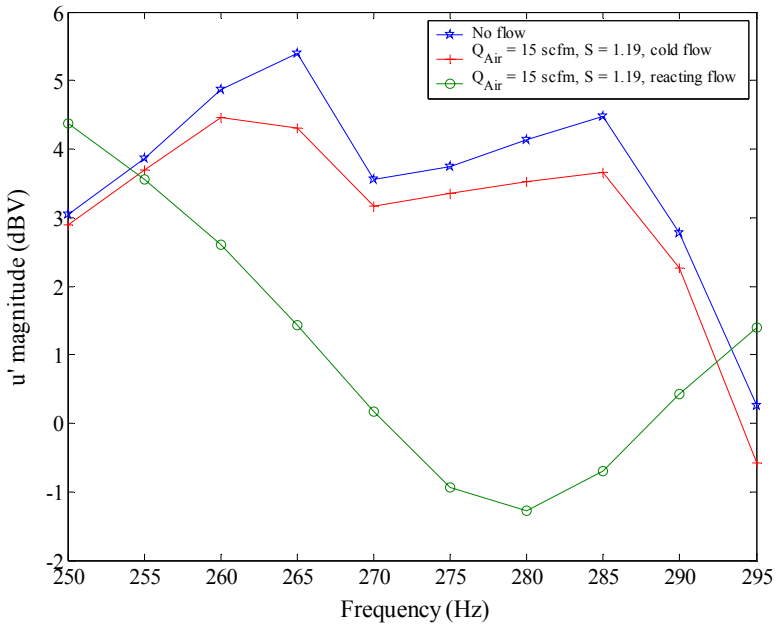

Figure 10.45: Power spectrum of u' between 250 and 295 Hz

nitude should increase the magnitude of the FRF by 4.8 dB, but Figure 10.46 shows that the increase in the FRF magnitude is about 11.5 dB, and the magnitude of the OH^* chemiluminescence very closely follows the behavior of the FRF magnitude. Thus, it is concluded that there is an increase in the OH^* chemiluminescence at the acoustic mode frequency, which is responsible for the prominent peaks seen in the results of the turbulent flame dynamic experiment. From the perspective of the systems level analysis, the above discussion indicates the presence of an unaccounted loop which communicates between the longitudinal acoustic characteristics of the combustor and the combustion process, as is schematically shown in Figure 10.47.

To investigate further and identify the unknown loop between the flame and the longitudinal acoustic characteristics, phase locked images of the flame were captured under various operating conditions using an ICCD camera. Figure 10.48 shows the unexcited flame at two operating conditions that differ only in equivalence ratio. Image (a) is of a flame for $Q_{Air} = 15$ scfm, $S = 1.19$ and $\Phi = 0.55$, while image (b) is of a flame for $Q_{Air} = 15$

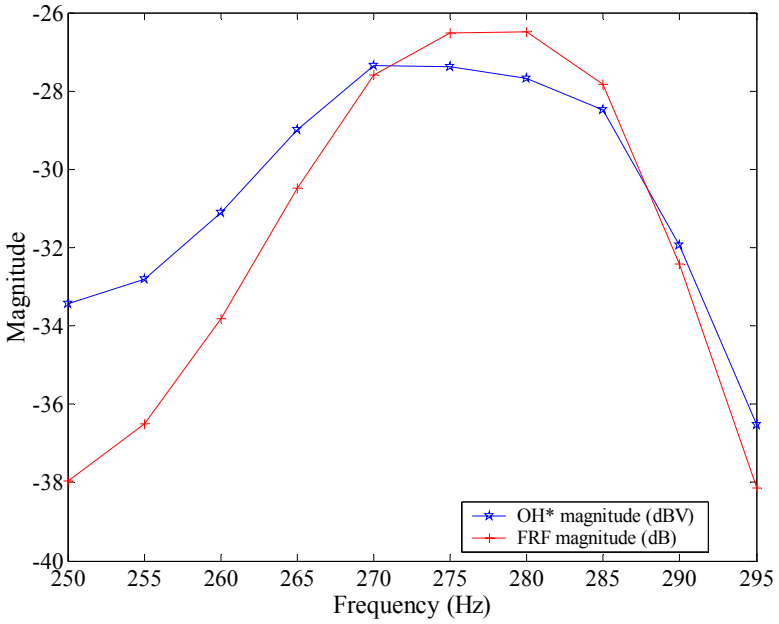

Figure 10.46: Power spectrum of OH^* signal and FRF (magnitude) for Q_{Air} = 15 scfm and $S = 1.19$, between 250 and 295 Hz

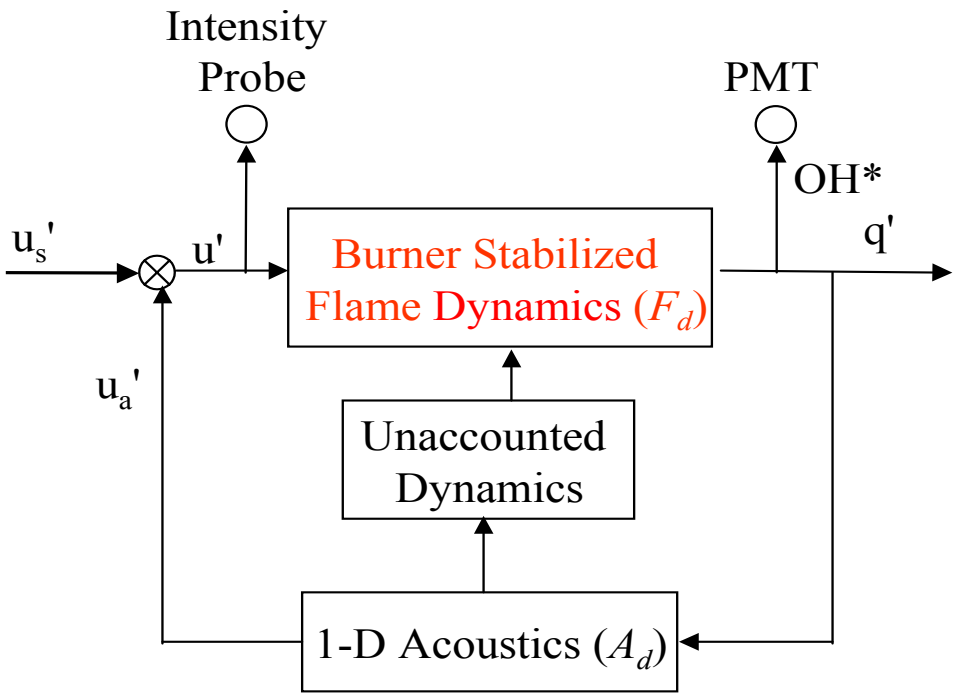

Figure 10.47: System level description of the turbulent swirl stabilized combustion process

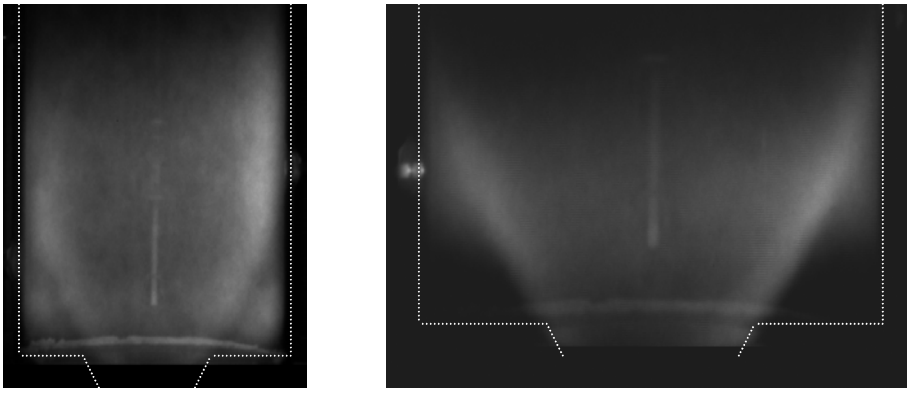

(a) (b)

Figure 10.48: (a) Image of swirl stabilized turbulent flame for $Q_{Air} = 15$ scfm, $S = 1.19$ and $\Phi = 0.55$, under steady burning conditions (b) Image of turbulent swirl stabilized flame for $Q_{Air} = 15$ scfm, $S = 1.19$ and $\Phi = 0.6$, under steady burning conditions

scfm, $S = 1.19$, and $\Phi = 0.6$. Both images indicate that the flame could be considered to be reasonably axi-symmetric. The images clearly demonstrate a slightly greater amount of burning occurring in the right half of the combustion chamber as compared to its left half. Apart from the minor skewness present in the profile at the inlet of the dump, inaccuracies in the alignment of the axis of the combustion chamber with that of the rest of the combustor could be responsible for the asymmetry observed in the flame. Nevertheless, there is a well defined burning process occurring on the shear layer between the two re-circulation zones.

Shown in Figure 10.49 are phased locked images taken at an excitation frequency of 275 Hz. The amplitude of excitation was maintained at the same level that was used for the dynamic experiments discussed earlier. The images do not show the presence of any coherent structures or vortex shedding process that influences the burning process, thus, eliminating the possibility of flow instabilities being the unknown factor that generated the second loop between the combustor acoustics and the heat release rate. The flame front resides almost entirely on the shear layer, but its surface area is changed during the cycle due to the radial expansion and contraction. This cyclical expansion and contraction is not phase locked

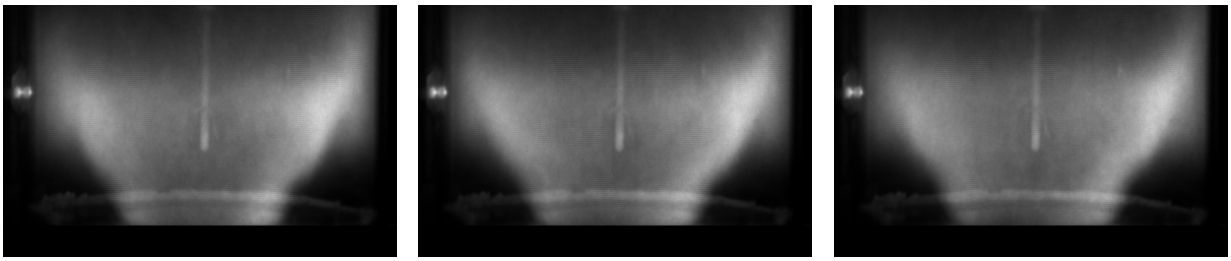

(a) 0° (b) 30° (c) 60°

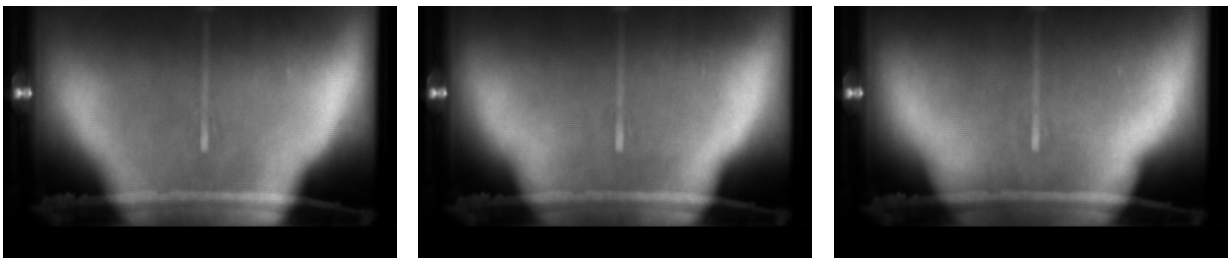

(d) 90° (e) 120° (f) 150°

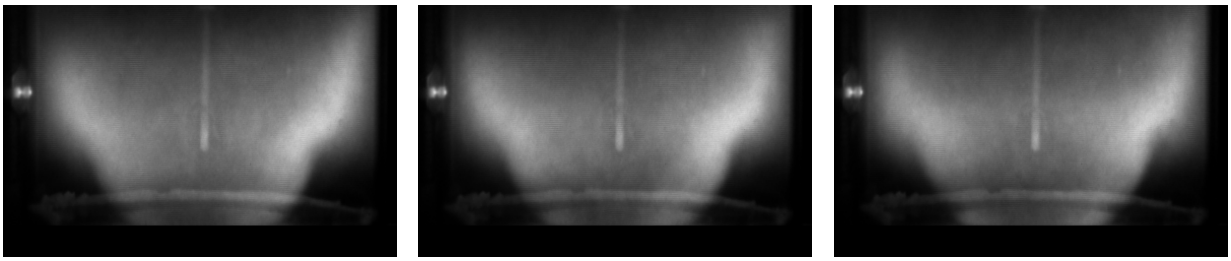

(g) 180° (h) 210° (i) 240°

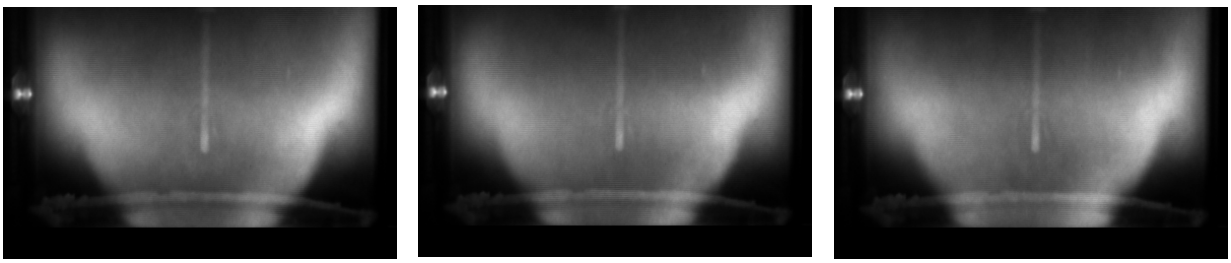

(j) 270° (k) 300° (l) 360°

Figure 10.49: Phase locked images of turbulent swirl stabilized flame for Q_{Air} = 15 scfm, S = 1.19 and Φ = 0.6, with excitation at 275 Hz

spatially along the axis of the combustor. Thus, over the entire cycle it generates an effect of a traveling wave.

Phased locked images at frequencies away from the acoustic modes of the combustor do not exhibit such a behavior, as is evident from Figure 10.50, where the flame was excited at a frequency of 105 Hz. The only effect observed in these images is the cycling of the overall intensity of the captured chemiluminescence. Thus, the response is spatially phase locked as is expected for a standing wave. Prior research [86, 87] has shown that the planar waves that are incident on a flame, do not remain planar within the reaction volume, but need to be treated as spherical waves. Interaction of the spherical acoustic wave with the temperature and density gradients present in the reaction volume, and the presence of a sudden area change in the flow direction result in the generation of evanescent waves in the radial and azimuthal direction. These evanescent waves decay in magnitude along the axial direction of the combustor and are primarily responsible for the generation of a traveling wave effect, as is seen from the images. It should be also noted that they are not present upstream and downstream of the reaction zone due to the absence of temperature gradients. Thus, the u' measurement technique used in the present research which records the velocity perturbation upstream of the flame, cannot account for the presence of these evanescent waves, although their effect on the heat release rate was measured by the OH^* chemiluminescence.

The above discussion leads to the conclusion that near field acoustic effects, which are at least two dimensional in nature, (axi-symmetric), are responsible for the excessive increase in the OH^* chemiluminescence and they need to be accounted for in the systems level description of the combustion process, so as to accurately predict the occurrence of thermo-acoustic instabilities.

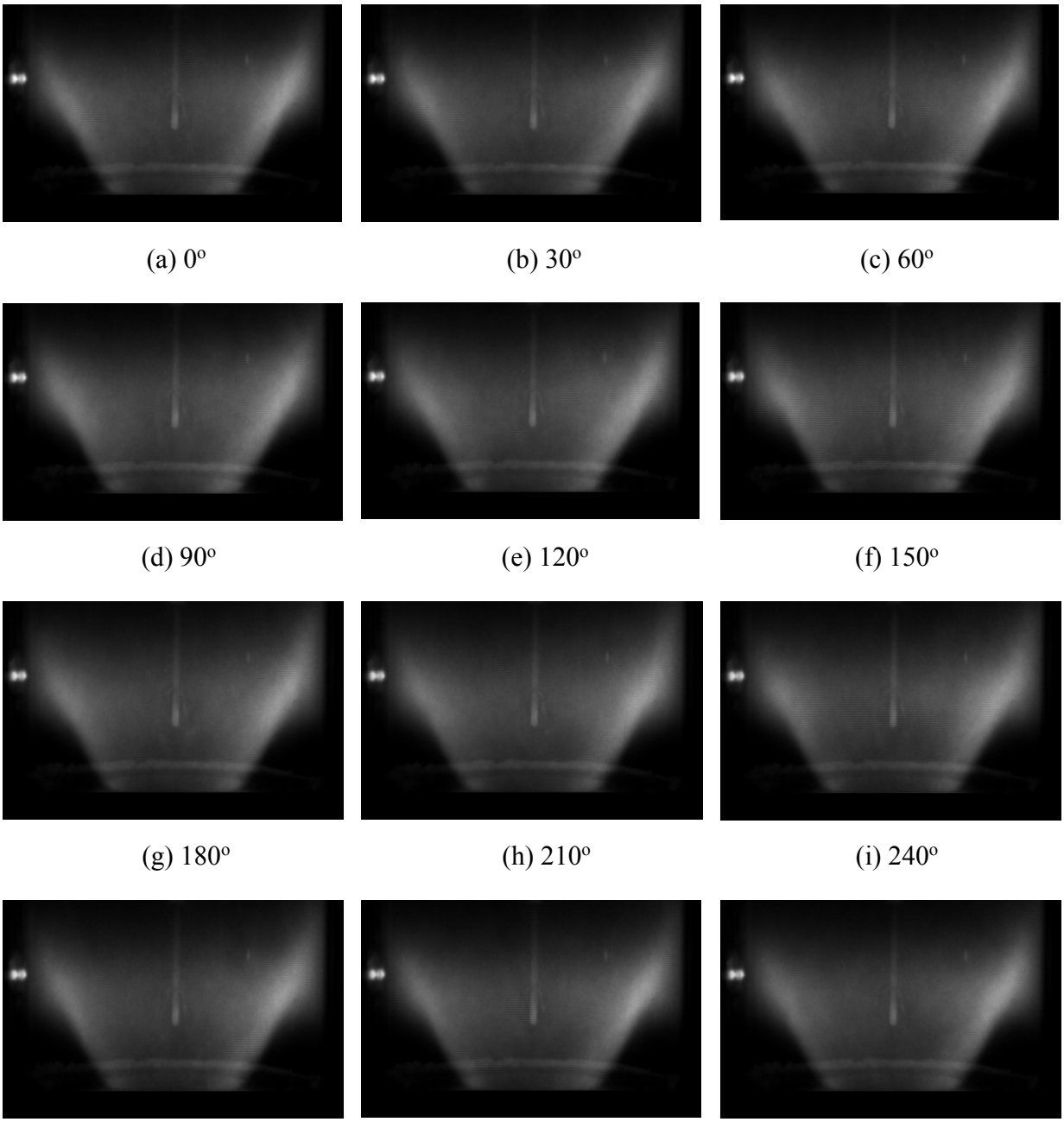

(a) 0° (b) 30° (c) 60°

(d) 90° (e) 120° (f) 150°

(g) 180° (h) 210° (i) 240°

(j) 270° (k) 300° (l) 360°

Figure 10.50: Phase locked images of turbulent swirl stabilized flame for Q_{Air} = 15 scfm, S = 1.19 and Φ = 0.6, with excitation at 105 Hz